

Photon-photon scattering in the resonance region at midrapidity at the LHC.*

RAINER SCHICKER

Phys. Inst., Heidelberg

MARIOLA KŁUSEK-GAWENDA, ANTONI SZCZUREK

Inst. Nucl. Phys., PAN Kraków, Univ. of Rzeszów

A study is presented to extend the measurements of photon-photon scattering in ultra-peripheral Pb-Pb collisions at the LHC into the mass region of the pseudoscalar resonances η and η' . The elementary photon-photon scattering cross section is presented. The cross section for photon-photon scattering in Pb-Pb is derived by convoluting the elementary photon-photon cross section with the Pb-Pb photon luminosity. The main background to two-photon final states, arising from double π^0 production with two of the four decay photons escaping detection, is examined, and possible kinematical conditions are discussed to optimize the signal-to-background ratio for such measurements at mid-rapidity.

PACS numbers: 25.20.Dc, 25.20.Lj

1. Introduction

Classical electrodynamics is epitomised by Maxwell's equations

$$\partial_\alpha F^{\alpha\beta} = \frac{4\pi}{c} J^\beta, \quad \partial_\alpha \mathcal{F}^{\alpha\beta} = 0. \quad (1)$$

The Maxwell equations in vacuum are linear in the electromagnetic fields \mathbf{E} and \mathbf{B} . Two electromagnetic waves will pass through each other without scattering. The superposition principle conveniently expresses the non-interaction of electromagnetic fields at the classical level. The electromagnetic field energy carried by the electron, however, poses a conceptual challenge at the classical level. Attempts to circumvent the infinite Coulomb

* Presented at Diffraction and Low-x Conference 2018, Reggio Calabria, Aug 26 - Sept 1

energy of a point charge resulted in Born-Infeld electrodynamics which affirms the linearity of Maxwell's equations down to some length scale intrinsic to the electron, and introduces non-linear equations for smaller lengths scales [1]. The polarisation of the vacuum in view of Dirac's positron theory led to the Euler-Kockel-Heisenberg Lagrangian which modifies the classical Maxwell's equation in vacuum by leading non-linear terms [2]. The advent of accelerating heavy-ions at the LHC has opened up the possibility of measuring the photon-photon scattering cross section due to the large associated photon luminosity of the heavy-ion beams. Evidence of such events have been reported by the ATLAS and CMS collaborations at the LHC [3, 4]. These measurements are, however, restricted to photon-photon invariant masses $W_{\gamma\gamma} > 5$ and 6 GeV for the CMS and ATLAS data, respectively. The purpose of the analysis presented here is to study the feasibility of measuring photon-photon scattering in the range $0.4 < W_{\gamma\gamma} < 5$ GeV. As a first step, we analyse the corresponding cross section in this range, and examine the background which is dominated by π^0 pair production with only two of the four decay photons being within the detector acceptance.

2. The elementary photon-photon scattering cross section

Different mechanisms contribute to the elementary $\gamma\gamma \rightarrow \gamma\gamma$ scattering.

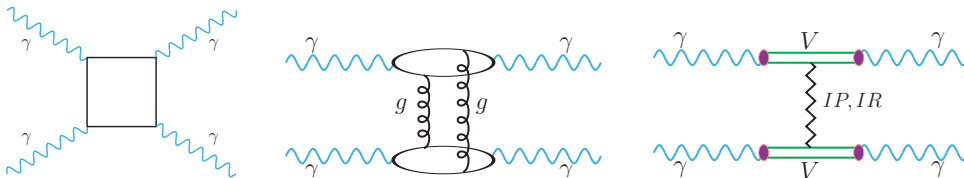


Fig. 1. Mechanisms of $\gamma\gamma \rightarrow \gamma\gamma$ scattering (Fig. taken from Ref. [5]).

In Fig. 1, the different mechanisms of $\gamma\gamma$ scattering are presented. On the left, the loop diagram for fermions, leptons and quarks, is shown. In the center, a QCD correction is displayed corresponding to a three-loop mechanism. On the right, the analogous process as expressed in the vector dominance approach is shown [5].

3. Photon-photon scattering in ultra-peripheral heavy-ion reactions

The cross section for photon-photon scattering in ultra-peripheral heavy-ion collisions can be calculated by folding the cross section of the elementary

mechanisms shown in Fig. 1 with the equivalent photon flux [6],

$$N(\omega, b) = \frac{Z^2 \alpha}{\pi^2} \frac{1}{\beta^2 b^2} \left| \int_0^\infty dv v^2 J_1(v) \frac{F_{el}(-\frac{u^2+v^2}{b^2})}{u^2+v^2} \right|^2. \quad (2)$$

The equivalent photon flux is defined in Eq. 2. Here, ω denotes the energy of the photon, and b represents the transverse distance from the center of the nucleus where the photon density is evaluated. The integral in Eq. 2 represents the form factor of the charge distribution of the source.

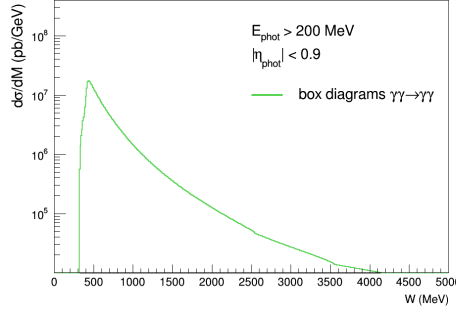


Fig. 2. Differential cross section $d\sigma/dM$ for photon scattering in PbPb-collisions.

The cross section for $\gamma\gamma \rightarrow \gamma\gamma$ in PbPb-collisions is calculated by convoluting the elementary cross section with the photon flux of Eq. 2,

$$\sigma_{PbPb \rightarrow PbPb\gamma\gamma}^{EPA} = \iint dn_\gamma^1 dn_\gamma^2 \sigma_{\gamma\gamma \rightarrow \gamma\gamma}(\omega_1, \omega_2). \quad (3)$$

The differential cross section for photon-photon scattering in PbPb-collisions at $\sqrt{s}=5.02$ TeV resulting from the convolution of Eq. 3 is shown in Fig. 2. This cross section is derived with the box diagrams of Fig. 1, and with conditions of the two final state photons being within the pseudo-rapidity range $|\eta| < 0.9$, and having an energy $E_{phot} > 200$ MeV.

4. Resonance signal from η, η' decays

The cross section for photoproduction of η, η' is taken according to [7]

$$\sigma_{\gamma\gamma \rightarrow R} = 8\pi(2J+1) \frac{\Gamma_{\gamma\gamma} \Gamma_{tot}}{(W^2 - M_R^2)^2 + M_R^2 \Gamma_{tot}^2}. \quad (4)$$

The cross section for photoproduction of η, η' in PbPb-collisions is calculated according to the convolution defined in Eq. 3.

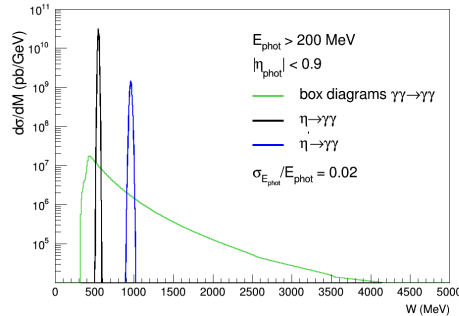


Fig. 3. Cross section for photoproduction of η, η' .

The η, η' cross section in PbPb-collisions at $\sqrt{s}= 5.02$ TeV multiplied by the branching ratio $\eta, \eta' \rightarrow \gamma\gamma$ is shown in Fig. 3. The values shown are derived with conditions of the two decay photons being within the pseudo-rapidity range $|\eta| < 0.9$, and having an energy $E_{phot} > 200$ MeV. The finite width of these two resonances results from the detector resolution of the photon measurements which is taken here to be $\sigma_{E_{phot}}/E = 0.02$.

5. Photoproduction of $\pi^0\pi^0$ pairs

The main background to the signal of two photons in the final state results from $\pi^0\pi^0$ production with two of the four decay photons escaping detection. The two measured photons from this $\pi^0\pi^0$ decay cannot be distinguished from the signal of photon-photon scattering.

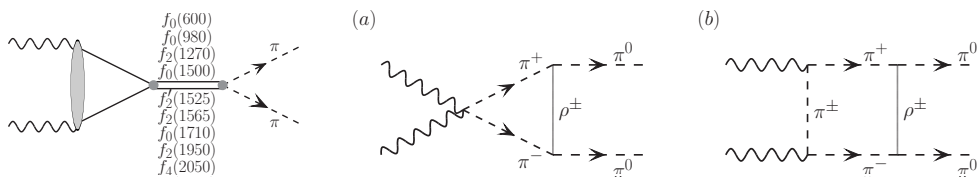


Fig. 4. Mechanisms of $\pi^0\pi^0$ photoproduction (Fig. taken from [8]).

The contribution of resonance decays to the $\pi^0\pi^0$ final state is shown in Fig. 4 on the left. Here, the resonances $\sigma(600)$, $f_0(980)$, $f_0(1500)$, $f_0(1710)$, $f_2(1270)$, $f_2(1525)$, $f_2(1565)$, $f_2(1950)$ and $f_4(2050)$ are considered [8]. The cross section $\gamma\gamma \rightarrow \pi^+\pi^-$ is much larger than for $\gamma\gamma \rightarrow \pi^0\pi^0$, hence even a small coupling between the charged and neutral pion channel might have an influence on the $\gamma\gamma \rightarrow \pi^0\pi^0$ cross section. Examples of processes leading to such channel couplings are shown in Fig. 4 in the middle and on the right.

6. Background from $\pi^0\pi^0$ decays

The $\pi^0\pi^0$ cross section in PbPb-collisions is calculated by convoluting the elementary $\pi^0\pi^0$ cross section with the photon flux according to Eq. 2. The background from $\pi^0\pi^0$ decays is shown in Fig. 5 by the solid red line. This background cross section is derived by the conditions that exactly one decay photon from each of the two π^0 's is within the pseudorapidity range $|\eta| < 0.9$, and that these photons have an energy $E_{\text{phot}} > 200$ MeV.

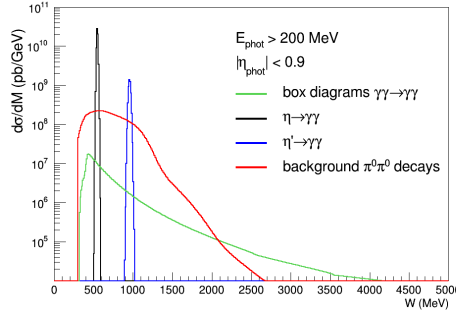


Fig. 5. Signal and background from $\pi^0\pi^0$ decays.

6.1. Background suppression by asymmetry cuts

The two photons of the signal are of equal transverse momentum and are back-to-back in azimuth. These correlations are smeared out due to finite resolution in the measurement of photon energy and azimuthal angle. The two photons from $\pi^0\pi^0$ decay do not show these correlations. A scalar (A_S) and vector (A_V) asymmetry can be defined for background suppression,

$$A_S = \frac{|\vec{p}_T(1)| - |\vec{p}_T(2)|}{|\vec{p}_T(1)| + |\vec{p}_T(2)|}, \quad A_V = \frac{|\vec{p}_T(1) - \vec{p}_T(2)|}{|\vec{p}_T(1) + \vec{p}_T(2)|}. \quad (5)$$

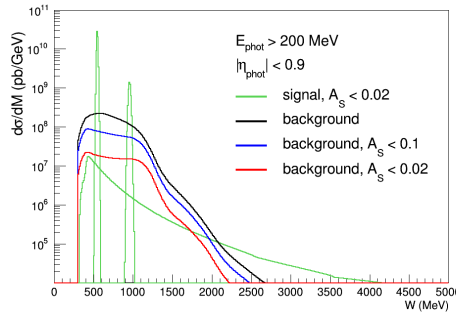


Fig. 6. Background suppression by asymmetry cut A_S .

The background reduction for condition $A_S < 0.1$ and $A_S < 0.02$ is shown in Fig. 6 by the blue and red line, respectively. The condition $A_S < 0.02$ reduces the background by about a factor ~ 10 while keeping 98% of the signal.

6.2. Background correction by sideband subtraction

The background remaining after the cut $A_S < 0.02$ can be subtracted by sideband correction. The signal band is given by $0.0 < A_S < 0.02$, with sideband 1 and 2 defined by $0.02 < A_S < 0.04$ and $0.04 < A_S < 0.06$, respectively. An estimator for the background in the signal region can be defined by linear extrapolation of the sidebands 1 and 2 into the signal region.

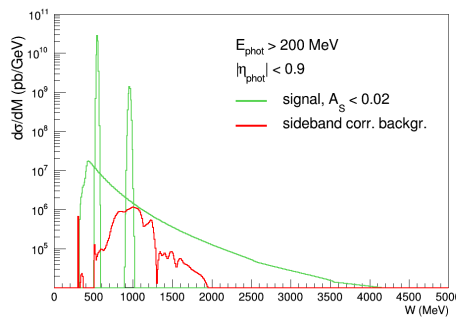


Fig. 7. Sideband corrected background.

The background remaining after sideband correction is shown in Fig. 7 by the red line. The sideband correction could be further improved by defining more than two sidebands, and by a non-linear extrapolation of the background into the signal region.

7. ACKNOWLEDGMENTS

This work is supported by the German Federal Ministry of Education and Research under promotional reference 05P15VHCA1.

REFERENCES

- [1] M.Born, Nature 132:3329 (1933) 282.
- [2] W.Heisenberg, H.Euler, Zeitschrift für Physik 98: 11-12 (1936) 714.
- [3] ATLAS Collaboration, Nature Phys. 13 (2017) no.9, 852.
- [4] CMS Collaboration, arXiv:1810.04602.
- [5] M.Khusek-Gawenda et al., Phys.Rev. C93 (2016), no.4, 044907.
- [6] G.Baur et al., Phys.Rept. 364 (2002) 359.
- [7] V.M.Budnev, I.F.Ginzburg, G.V.Meledin, V.G.Serbo, Phys.Rept.15, (1975) 181.
- [8] M.Khusek-Gawenda, A.Szczurek, Phys.Rev. C87 (2013), no.5, 054908.